Journal of Hazardous Materials 398 (2020) 122945

Contents lists available at ScienceDirect

Journal of Hazardous Materials

journal homepage: www.elsevier.com/locate/jhazmat

Biochemical synthesis of palladium nanoparticles: The influence of chemical fixatives used in electron microscopy on nanoparticle formation and catalytic performance

Ling Tan[a,b,*], Thomas Ray Jones[b], Jordan Poitras[b], Jianping Xie[a], Xinxing Liu[a], Gordon Southam[b]

[a] School of Minerals Processing and Bioengineering, Central South University, Changsha, Hunan 410083 China
[b] School of Earth & Environmental Sciences, The University of Queensland, St. Lucia, QLD 4072 Australia

GRAPHICAL ABSTRACT

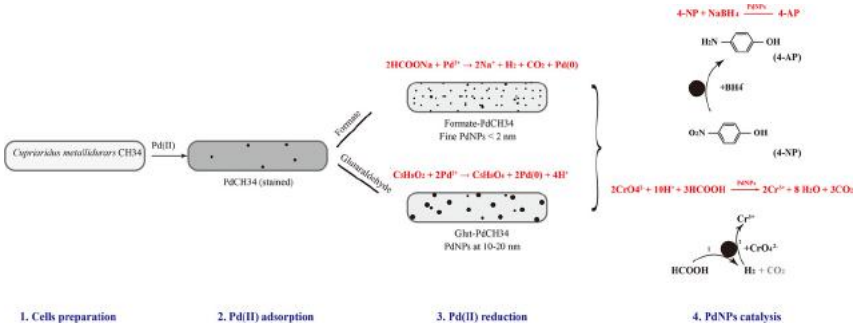

ARTICLE INFO

Editor: L. Eder

Keywords:
Biosynthesis
Palladium nanoparticles
Chemical fixatives
Catalytic performance

ABSTRACT

Palladium nanoparticles (PdNPs) can catalyse a range of reductive chemical reactions transforming both organic and inorganic environmental pollutants. PdNPs that ranged from < 2 to 2–40 nm were synthesized using chemical methods, and bacterial biomass with/without chemical fixatives. PdNP formation was enhanced by adsorption of Pd(II) to bacterial biomass, followed by fixation with formate or glutaraldehyde. TEM-SAED analyses confirmed that the cell associated PdNPs were polycrystalline with a face-centered cubic structure. Chemically formed PdNPs possessed a higher Pd(0):Pd(II) ratio and produced structurally similar nanoparticles as the biotic systems. These PdNPs were employed to catalyze two, reductive chemical reactions, transforming 4-nitrophenol (4-NP) and hexavalent chromium [Cr(VI)], into 4-aminophenol and Cr(IV), respectively. In the reduction of 4-NP, the catalytic performance was directly proportional to PdNP surface area, *i.e.,* the smallest PdNPs in formate-PdCH34 cells had the fastest rate of reaction. The mass of Pd(0) as PdNPs was the main contributor to Cr(VI) reduction; the chemically synthesized PdNPs showed the highest removal efficiency with 96% at 20 min. The use of glutaraldehyde enhanced the reduction of Pd(II) and promoted PdNPs formation, *i.e.,* creating an artefact of fixation; however, this treatment also enhanced the catalytic performance of these PdNPs.

* Corresponding author at: School of Minerals Processing and Bioengineering, Central South University, Changsha, Hunan 410083, China.
E-mail address: TanLing@csu.edu.cn (L. Tan).

https://doi.org/10.1016/j.jhazmat.2020.122945
Received 25 February 2020; Received in revised form 9 May 2020; Accepted 10 May 2020
Available online 17 May 2020
0304-3894/

1. Introduction

Palladium (Pd) is a significant precious metal that has been applied in many industries such as catalyst, chemical, electronic, and glass (Froehlich et al., 2017). As one of the main components of automobile catalysts, the Pd emission in exhaust gas has resulted to the release of Pd into the environment, as airborne particulate matter (Tilch et al., 2000), road and tunnel dust (Leśniewska et al., 2004), sewage sludge (Leopold et al., 2008), and soil taken from areas of high traffic density (Leopold et al., 2017). The consumption of Pd and its increasing demand has led to a parallel increase in Pd price (Tan et al., 2017). Hence, it is essential to improve the efficient use and effectiveness of Pd materials.

PdNPs have received significant attention in recent years for their superior catalytic performance in reduction, oxidation and C−C coupling reactions (Li et al., 2015). These properties are due to the advantages of high surface-area-to-volume ratio, highly ordered structure and densely populated unsaturated surface coordination sites (Ncube et al., 2015). Palladium ions can be reduced to zero-valent nanoparticles by physicochemical methods, such as the sonochemical, electrochemical and wet chemistry methods (Saldan et al., 2020). Unfortunately, such nano-dimensional materials (in the 1−100 nm size domain) are generally unstable because of their large active surface area, resulting in self-aggregation, and thus the reduction of catalytic activity (Wu et al., 2013; Yuan et al., 2010). A variety of stabilisers including organic ligands, salts/surfactants, polymers and dendrimers are typically introduced during the chemical formation of PdNPs (Cookson, 2012), generating undesirable waste streams (Yates et al., 2013). In some cases these surfactants can also form strong chemical bonds on the surface of PdNPs severely limiting their catalytic potential (Chen et al., 2011; Mazumder and Sun, 2009).

Alternatively, the biological synthesis of nanoparticles utilizing microorganisms is a simple, inexpensive, and environmentally benign method to obtain nanoparticles of high mono dispersity. The bacteria can serve as a stabiliser and disperser to circumvent the aggregation of nanoparticles (Xu et al., 2018). Both living and dead microbial biomass can produce intracellular or extracellular inorganic nanoparticles (De Windt et al., 2006; Lengke et al., 2007; Windt et al., 2005; Yates et al., 2013). *Plectonema boryanum* UTEX 485 (Lengke et al., 2007), *Shewanella oneidensis* MR-1 (Xu et al., 2018), *Escherichia coli* (Mikheenko et al., 2016) and *Desulfovibrio desulfuricans* (Bennett et al., 2013; Creamer et al., 2007), *Enterococcus faecalis* (Cui et al., 2017) and *Bacillus sphaericus* (Creamer et al., 2007) have been reported to adsorb Pd (II) and synthesize PdNPs in their bacterial biomass. The metal-resistant bacterium - *Cupriavidus metallidurans* CH34 (*C. metallidurans* CH34) harbours plasmids enabling detoxification of various heavy metals, including Ni(II), Co(II), CrO_4^{2-}, Hg(II), Ag(I), Cd(II), Cu(II) and Pb(II) (Monchy et al., 2007). *C. metallidurans* CH34 can also form gold (Montero-Silva et al., 2017; Srivastava and Mukhopadhyay, 2015), platinum (Campbell et al., 2018) and silver (Ledrich et al., 2005) nanoparticles in cells, however, the formation of PdNPs using this strain and reductants have not been fully studied.

Whole cells with PdNPs could potentially be used as catalysts for promoting remediation reactions of environmental pollutants, *i.e.,* the reduction of 4-nitrophenol (4-NP) to 4-aminophenol (4-AP) and the reduction of Cr(VI) to Cr(III). 4-NP, a pollutant toxic to aquatic life and human health (Le et al., 2014), is a widely used chemical for the synthesis of pharmaceutical products, dyes and explosives (Le et al., 2015). The catalytic reduction of the nitro group using metal nanoparticles is expected to be the most efficient, green, and economical method for reducing 4-NP toxicity (Chiou et al., 2013). Cr(VI) is a highly toxic agent that is carcinogenic, mutagenic and teratogenic to organisms (Gao et al., 2018). It is a by-product of industrial operations, which include metallurgy, leather tanning and pigment manufacturing (Gao et al., 2018). In contrast, Cr(III) (as $Cr(OH)_{3(s)}$) is less toxic and less mobile in nature, and trace amounts of Cr(III) are recognized as an essential nutrient for some organisms (Dai et al., 2018). The reduction of Cr(VI) to Cr(III) can be catalysed by nanoparticles and is, therefore, an excellent option for toxic Cr(VI) remediation (Celebi et al., 2016).

Bacterial ultra-thin sections are commonly used for intracellular nanoparticle observation, however, the influence of chemical fixatives on nanoparticles' formation and their catalytic performance was previously unknown. In this study, PdNPs with different sizes were synthesized using *C. metallidurans* CH34 cells with and without formate or glutaraldehyde (glut) as fixatives (chemical reductants). The morphological and structural characteristics of PdNPs synthesized by both chemical and biological methods were analysed using scanning electron microscopy (SEM), transmission electron microscopy (TEM) and X-ray photoelectron spectroscopy (XPS). Additionally, the catalytic performance of different PdNPs for the reduction of 4-NP and Cr(VI) was examined using ultraviolet to visible spectroscopy.

2. Materials and methods

2.1. Bacterial culture

Cupriavidus metallidurans CH34 (ATCC®43123) was acquired from the American Type Culture Collection in Manasssas, VA, USA. Cells were propagated from an agar plate colony in 100 mL Difco™ nutrient broth (BD Co., USA) at 30 °C and 120 rpm for 12 h on a shaker table. Then, 20 µL of culture was inoculated to 100 mL fresh nutrient broth for another 12 h under the same conditions (Campbell et al., 2018). The culture was centrifuged at 11,200 x g for 10 min to form a pellet, then washed twice with Milli-Q water under the same conditions, *i.e.,* blank CH34 cells.

2.2. Palladium (II) adsorption and reduction

To get a suspension of OD_{600} = 1.758 (equivalent to 20 g wet biomass per litre), a suitable amount of Milli-Q water was added to the washed bacterial pellet. Sixty mL of bacterial suspension was added to 60 mL of 1.45 mM (154 mg/L) Pd(II) solution to get a final bacterial concentration of 10 g/L and a Pd (II) concentration of 0.72 mM (77 mg/L). Samples were covered with aluminium foil to prevent photochemical reduction and shaken at 120 rpm at 30 °C. After 3 h incubation, the bacterial suspensions were equally divided into the three groups and centrifuged at 11,200 × *g* for 10 min; the supernatant was then acidified to a volume of 2% nitric acid. The supernatant was sent to Australian Laboratory Services (ALS), Brisbane, Australia, and examined using inductively coupled plasma mass spectrometry (ICP-MS) analysis with a detection limit of 0.001 mg/L. For Pd(II) reduction, cells possessing adsorbed-Pd were washed twice with Milli-Q water at 11,200 x g for 5 min, and the pellets were used for three different treatments (54% of the Pd (II) [41.34 mg] adsorbed to 10 g wet biomass):

- PdCH34 pellet, no further treatment. The viability of PdCH34 cells was determined by fluorescent microscopy using LIVE/DEAD® BacLight™ bacterial viability kits (L-7012, Molecular Probes, Inc., Eugene, Oregon).
- Formate-PdCH34 (De Windt et al., 2006), 40 mL of degassed sodium formate (25 mM) was added to the bacterial pellet and transferred to serum bottles. The solution was flushed with N_2 for 1 h to drive off the dissolved O_2, then sealed with butyl rubber stoppers, covered with Al foil, and agitated on a shaker table for 12 h at 120 rpm and 30 °C. After 12 h, the cells were collected and washed twice with Milli-Q water (11,200 × *g* for 5 min).
- Glutaraldehyde treatment (glut-PdCH34), two mL of 250 mM glutaraldehyde ($2.5\%_{(aq)}$) was used to fix the bacterial pellet in the dark (to prevent photochemical reactions) without agitation. After 12 h, the cells were collected and washed twice with Milli-Q water (11,200 × *g* for 5 min).

Formate (a monovalent fixative) and glutaraldehyde (a divalent fixative) were used as chemical controls: 20 mL volumes possessing 0.78 mM Pd(II) solution (to match the amount of Pd(II) that was adsorbed + precipitated by the bacteria) was added to 20 mL 50 mM degassed formate and to 20 mL of 500 mM glutaraldehyde (5.0% $_{(aq)}$) under the same reaction conditions as biotic experiments. The PdNPs in formate and glutaraldehyde chemical controls were collected and washed twice with Milli-Q water at 11,200 × *g* for 10 min.

2.3. Scanning electron microscopy

2.3.1. Sample preparation

The blank, formate- and glut-PdCH34 cells prepared as mentioned above were further fixed with 2 mL of 250 mM glutaraldehyde overnight to ensure preservation of the cells (note, no new nanoparticles were observed). Fixed bacteria were dehydrated using a series of 20, 40, 60, 80 and 2 × 100% ethanol solutions with samples being treated for 15 min at each concentration. The chemical drying agent hexamethyldisilizane (HMDS) was used to dry the cells after ethanol dehydration. A series of mixed solutions with HMDS:absolute ethanol in ratios of 1:2, 2:1 and 100% HMDS were added with 20 min incubations.

For secondary electron SEM, HMDS cell suspensions were dropped onto silicon wafers and dried at 40 °C overnight under vacuum. The samples were then plasma cleaned using an Evactron ZephyrTM Plasma Cleaner (XEI Scientific, USA) before imaging. For energy-dispersive X-ray analysis (EDS), cell powders (after HMDS treatment) were placed onto carbon tape, plasma cleaned and carbon-coated (10 nm) before imaging.

2.3.2. SEM observation and EDS analysis

A JEOL 7800 SEM, operated at 1 kV and a 6 mm working distance with an upper secondary electron detector was used for obtaining high-magnification images without coating the samples. A JEOL 7001 SEM was used for EDS analysis operating at 10 kV and a working distance of 10 mm.

2.4. Transmission electron microscopy

2.4.1. Whole-mount cells observation

A micropipette tip was used to sample blank, PdCH34, formate-PdCH34 and glut-PdCH34 cells, and then the bacteria were suspended in a drop of Milli-Q water. Twenty µL of suspension was dropped to Formvar carbon-coated 200-mesh gold grids (ProSciTech Pty. Ltd., Australia) and incubated for 10 min at room temperature to allow for bacterial attachment. Grids were dipped in filter-sterilized Milli-Q water five times to remove any salt, then air-dried prior to microscopy. Whole-mount cells were imaged using a Hitachi HT7700 transmission electron microscope operating at 80 kV. The sizes of the PdNPs were measured using ImageJ software.

2.4.2. Ultra-thin sections

Blank CH34 and formate-PdCH34 were fixed overnight using 2 mL of 250 mM glutaraldehyde, no additional glutaraldehyde was added to the glut-PdCH34. Cells were pelleted by centrifugation (3000 × *g*) to decant the glutaraldehyde, and the pellets embedded in 2% (w/v) noble agar (Difco Laboratories). The agar was then cut into small blocks and dehydrated using a 50%, 70%, 90% and 2 × 100% ethanol series in a microwave (PELCO BioWave® Microwave Processor, Ted Pella Inc.) for 40 s at 250 W without vacuum. The resin infiltration was done by slowly replacing the ethanol with EMS epoxy resin, the agar blocks were incubated in a series of resin mixtures (resin:ethanol = 1:2, 1:1, 2:1 and 2 × 100% resin) in a Biowave microwave for 3 min each at 250 W under low vacuum. The samples were transferred to silicone molds with 100% resin overnight for polymerization. Embedded samples were ultra-thin sectioned using a Leica Ultracut UC6 microtome (Leica, Austria) equipped with a diamond knife to a thickness of 100 nm and collected on carbon-coated 100-mesh copper grids (Campbell et al., 2018). The high-resolution transmission electron microscopy (HRTEM), high-resolution high-angle annular dark field-scanning transmission electron microscopy (HAADF-STEM), and the selected area electron diffraction (SAED) were performed on the Philips Tecnai FEI F20 FEG-STEM at 200 kV.

2.5. X-ray photoelectron spectroscopy

The PdNPs in the glutaraldehyde chemical control, PdCH34, and formate- and glut-PdCH34 cells were freeze-dried for XPS analyses. Data was acquired using a Kratos Axis ULTRA X-ray Photoelectron Spectrometer incorporating a 165 mm hemispherical electron energy analyser. The incident radiation was monochromatic Al Kα X-rays (1486.6 eV) at 150 W (15 kV, 10 ma). Survey (wide) scans were taken at an analyzer pass energy of 160 eV and multiplex (narrow) high-resolution scans at 20 eV. Survey scans were carried out over 1200 − 0 eV binding energy range with 1.0 eV steps and a dwell time of 100 ms. Narrow high-resolution scans were run with 0.05 eV steps and 250 ms dwell time. Base pressure in the analysis chamber was 1.0×10^{-9} torr and during sample analysis 1.0×10^{-8} torr. The obtained spectra were referenced to C 1s peak at 284.8 eV assigned to the adventitious carbon for all samples. Atomic concentrations were calculated using the CasaXPS version 2.3.14 software and a Shirley baseline with Kratos library Relative Sensitivity Factors (RSFs). Peak fitting of the high-resolution data was also carried out using the CasaXPS software.

2.6. PdNPs catalytic performance in 4-NP and Cr(VI) reduction

The chemically formed PdNPs, blank cells, PdCH34, formate-PdCH34, and glut-PdCH34 cells were freeze-dried and used for 4-NP and Cr(VI) reduction. To analyse the catalytic performance of chemically formed PdNPs, 0.4 mg of PdNPs from the glutaraldehyde chemical control was added to 5 mL Milli-Q water. In this study, the ratio of wet weight:dry weight of *C. metallidurans* CH34 was 10:0.4525, and 0.39 mM (41.34 mg) of Pd (II) was adsorbed by 10 g wet biomass (equivalent to 91.36 mg/g dry biomass). Therefore, 4.3 mg of blank cells, 4.7 mg of PdCH34 cells, formate- and glut-treated cells were added to 5 mL Milli-Q water to compare the PdNPs performance with the same amount of chemically formed PdNPs. All samples were sonicated in ultrasonic washer for 60 min to distribute PdNPs and PdNP-loaded cells. For 4-NP reduction (Xu et al., 2018), 250 µL of 1000 µM 4-NP, 720 µL of Milli-Q water and 30 µL PdNPs or PdNP-loaded cells were added and mixed in a cuvette, the degradation was initiated by adding 1000 µL of 10 mM sodium borohydride. The 30 µL PdNPs or PdNP-loaded cells was replaced with 30 µL Milli-Q water in blank control to eliminate the background of 4-NP reduction. The absorbance was measured in 2, 4, 6, 8, 10, 15, 30, 45 and 110 min using a UV–vis Spectrophotometer (ThermoFisher Scientific, US) between 250 − 600 nm, and the absorbance at the 400 nm wavelength was used for the calculation of remove efficiency. Cr(VI) reduction (Ng et al., 2019) was conducted in 4-(2-Hydroxyethyl)piperazine-1-ethanesulfonic acid (HEPES) buffer system to maintain an neutral pH [35]. Specifically, 1000 µL of 2000 µM Na_2CrO_4 (in 30 mM HEPES buffer), 770 µL of 30 mM HEPES buffer and 30 µL of PdNPs or PdNP-loaded cells were added and mixed in a cuvette, and the reaction was initiated by adding 200 µL 10% formic acid. Likewise, the 30 µL PdNPs or PdNP-loaded cells was replaced with 30 µL Milli-Q water in blank control to eliminate the background of Cr(VI) reduction. The absorbance was measured at 1, 10, 20, 30, 40, 50, 60, 120, 330 and 1320 min between 250 − 600 nm. The Cr(VI) removal efficiency were calculated according to the absorbance at a wavelength of 362 nm using the following equation:

$$\text{Remove efficiency (\%)} = (A_0 - A_t)/A_0$$

Where A_0 is the absorbance at time 0, A_t is the absorbance at time t.

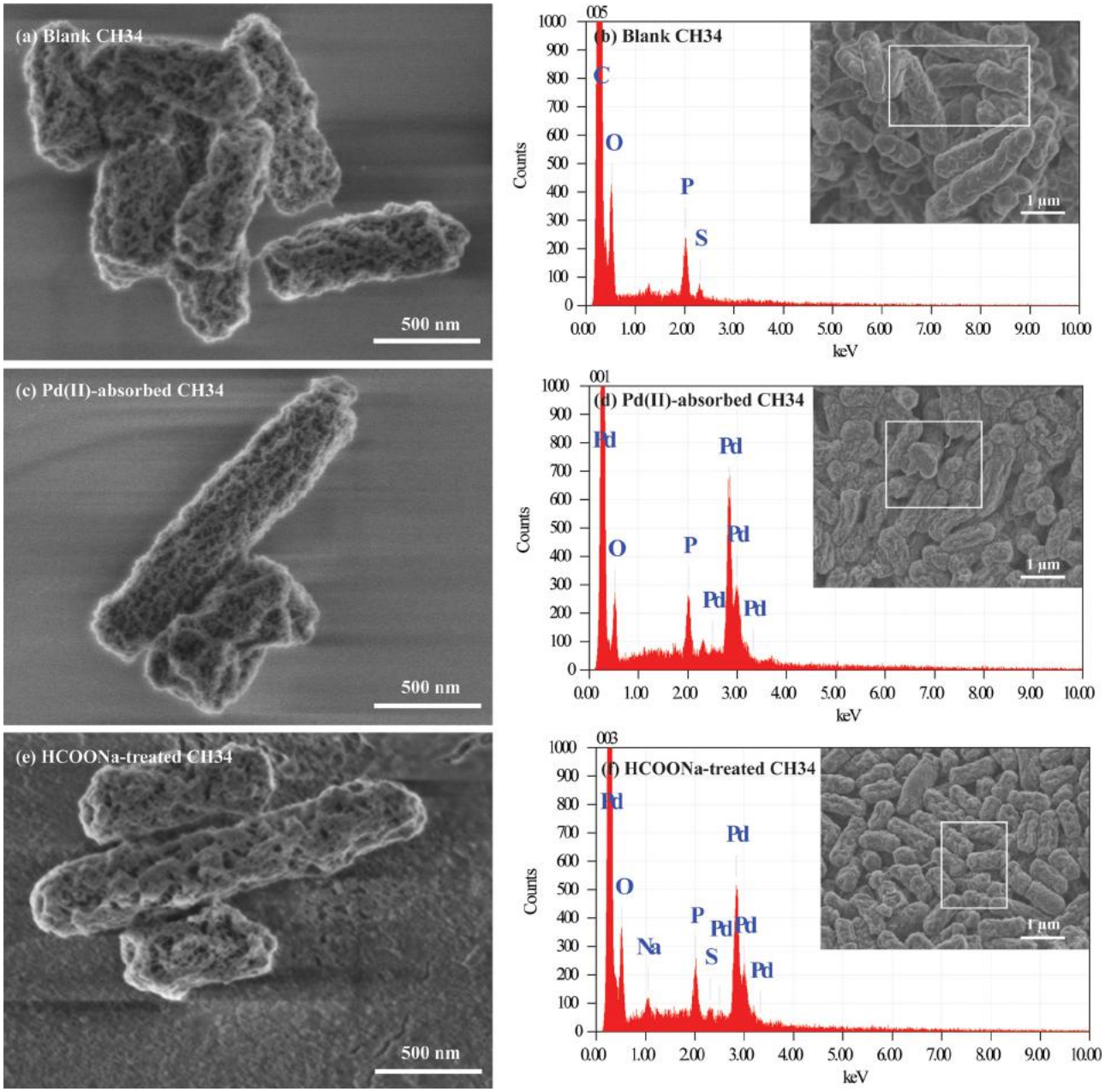

Fig. 1. Secondary electron SEM micrographs and EDS analysis for blank CH34 cells (a,b), formate-PdCH34 cells (c,d) and glut-PdCH34 cells (e,f).

3. Results and discussion

3.1. SEM-morphological characteristics

The morphological characteristics before and after Pd(II) reduction are shown in Fig. 1. In this SEM analysis, glutaraldehyde fixation, ethanol series dehydration, and HMDS drying were used for sample preparation, which has been shown to preserve the morphology of extracellular polymeric substances, and reduce cell distortion and shrinkage (Lee and Chow, 2012). Because it was not fixed, the PdCH34 sample was omitted from the SEM observations. After Pd(II) adsorption and reduction, the CH34 cells remained structurally intact (Fig. 1). The blank CH34, and formate and glut-PdCH34 cells were morphologically similar. While no PdNPs were observed on the surface of the bacterial cells in this study, spherical Pd-Pt NPs were observed on the cell envelope of *Shewanella oneidensis* MR-1 in a similar project (Xu et al., 2018). The EDS spectrum confirmed the uptake of Pd in formate- and glut−CH34 (Fig. 1d and f) in comparison to blank CH34 cells (Fig. 1b). Ion exchange in bacterial cell envelopes is believed to be the main mechanism for bacterial adsorption (Feng et al., 2007), however, the dispersal of PdNPs throughout the cytoplasm suggests that adsorption can occur throughout the cells.

3.2. TEM-PdNPs in whole bacterial cells

PdNPs in the glutaraldehyde chemical control, PdCH34, and formate- and glut-treated cells were examined using TEM. The formate chemical control solution began with a brownish colour then became transparent overnight (Fig. 2b); this could be attributed to the reduction of Pd(II) and aggregation of Pd(0) nanoparticles (Fig. 2a). In the glutaraldehyde control, the solution became dark brown after reacting with Pd(II) overnight. TEM whole mounts (Fig. 2c) demonstrate that the dendrite-shaped PdNPs formed were generally homogeneous in size, ranging from 20 − 40 nm with an average size of 34.3 ± 8.1 nm;

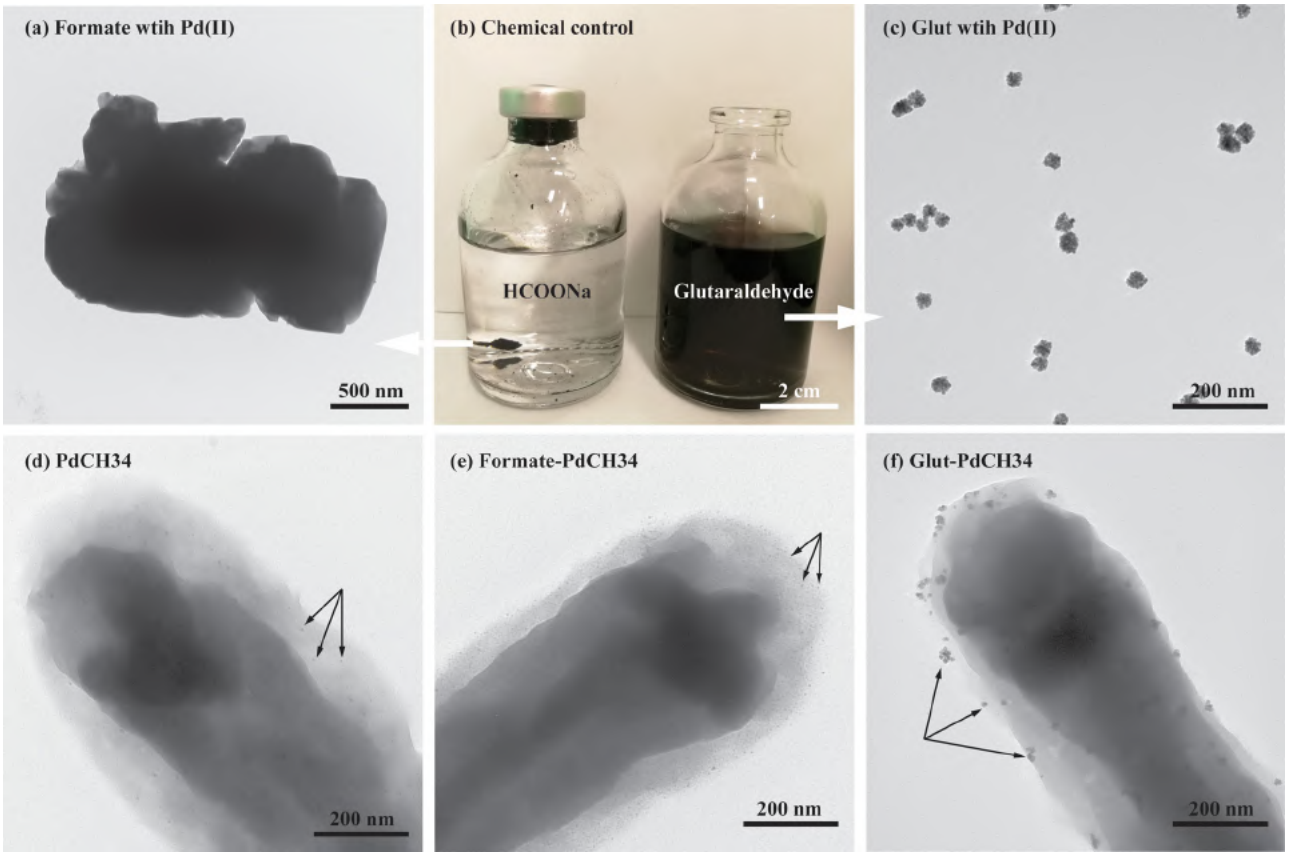

Fig. 2. TEM whole mounts and light micrographs of PdNPs in chemical controls and different CH34 cells. (a) TEM image for PdNPs formed in formate chemical control; (b) photographs of an aged formate and a glutaraldehyde chemical control; (c) TEM image for PdNPs in glutaraldehyde chemical control; (d) TEM image for PdCH34 whole-mount cells; (e) TEM image for formate-PdCH34 whole-mount cells; (f) TEM image for glut-PdCH34 whole-mount cells.

however, after one week, the glutaraldehyde solution particles formed aggregated grains (data not shown). After Pd(II) adsorption and reduction, PdCH34 cells were stained with a few PdNPs with size of ca. 5 nm shown in the whole-mount image (Fig. 2d). In contrast, the formate-PdCH34 cells had a greater number of fine, black (electron-dense) nanoparticles (< 2 nm) enriched in the cell envelope, while the cytoplasm remained stained (Fig. 2e). After glutaraldehyde reduction, small dendrite-shaped PdNPs similar to the glutaraldehyde chemical control were observed, ranging from $10-20$ nm with an average size of 12.4 ± 4.2 nm (Fig. 2f); the cells were still stained when compared with blank CH34. PdNP size is related to the atomic mass of the reductant(s) or dispersing agents; the binding affinity between Pd(II) and reductant; and lastly, the speed of PdNPs nucleation and growth (Wang et al., 2012). Therefore, the larger molecule size combined with the slower reactivity of glutaraldehyde to Pd(II) could contribute to slower PdNP crystallization, leading to larger PdNPs in comparison to that of formate-treated cells. Compared with the chemical controls, the bacterial cells acted as a dispersing agent, forming small PdNPs and preventing self-aggregation. Furthermore, the high Pd(II) concentration (0.72 mM) in the absence of food, *i.e.*, in buffer led to the death of cells (visualized using Bac-Light™ fluorescent microscopy, data not shown), which was consistent with De Windt et al. (2006) who reported that planktonic bacterial cells substantially lose viability when exposed to > 0.47 mM Pd(II). These non-viable bacterial cells acted as both a complex of functional groups for Pd(II) adsorption as well as an electron donor for Pd(II) reduction.

Chemically, dispersed PdNPs can be formed in sodium formate aqueous solution when catalysed by citric acid [$2HCOONa + Pd^{2+} = 2Na^{+} + H_{2(g)} + CO_{2(g)} + Pd(0)_{(s)}$] (Wang et al., 2012). In this experiment, the bacterial (cytoplasm) would contain an abundance of low molecular weight, *e.g.*, tricarboxylic acid cycle intermediates, and high atomic mass polymers that could promote Pd-reduction. In the well-sealed serum bottles/anaerobic conditions employed in this study, H_2 could further serve as an electron donor for Pd(II) reduction (Windt et al., 2005); open, formate-reducing systems (loss of H_2) remained brownish, producing less PdNPs than the sealed systems.

Glutaraldehyde was introduced as a fixative for electron microscopy in 1963 (Sabatini et al., 1963), and bacterial thin sections were considered a direct and powerful way to visualize the nanoparticles inside cells (Bennett et al., 2013; De Windt et al., 2006; Deplanche et al., 2010; Ng et al., 2019). However, the glutaraldehyde chemical control and glut-PdCH34 demonstrated that glutaraldehyde could reduce Pd(II) into Pd(0) and form PdNPs. The following two-step mechanism was proposed for Pd(II) binding and reduction by glutaraldehyde:

1 Pd(II) binding: the commercial glutaraldehyde solution contains hemihydrate, dihydrate and the cyclic hemiacetal (Whipple and Ruta, 1974); the hydroxyl in these chemicals could contribute to the Pd(II) binding/extraction via ion exchange.
2 Pd(II) reduction: glutaraldehyde could slowly decompose to form glutaric acid in an aqueous system because of the O_2 oxidation (Coupland and Hopwood, 1966; Gillett and Gull, 1972). Similarly, it could happen using Pd(II) as oxidizer: [$C_5H_8O_2 + 2Pd^{2+} = C_5H_8O_4 + 2Pd(0)_{(s)} + 4H^{+}$], the carboxyl in glutaric acid provides another ideal functional groups for Pd(II) adsorption by ion exchange.

3.3. HRTEM-PdNPs structure in bacterial thin sections

HAADF-STEM with EDX was used to confirm the structure of PdNPs inside formate- and glut-PdCH34. Thin sections of formate−CH34

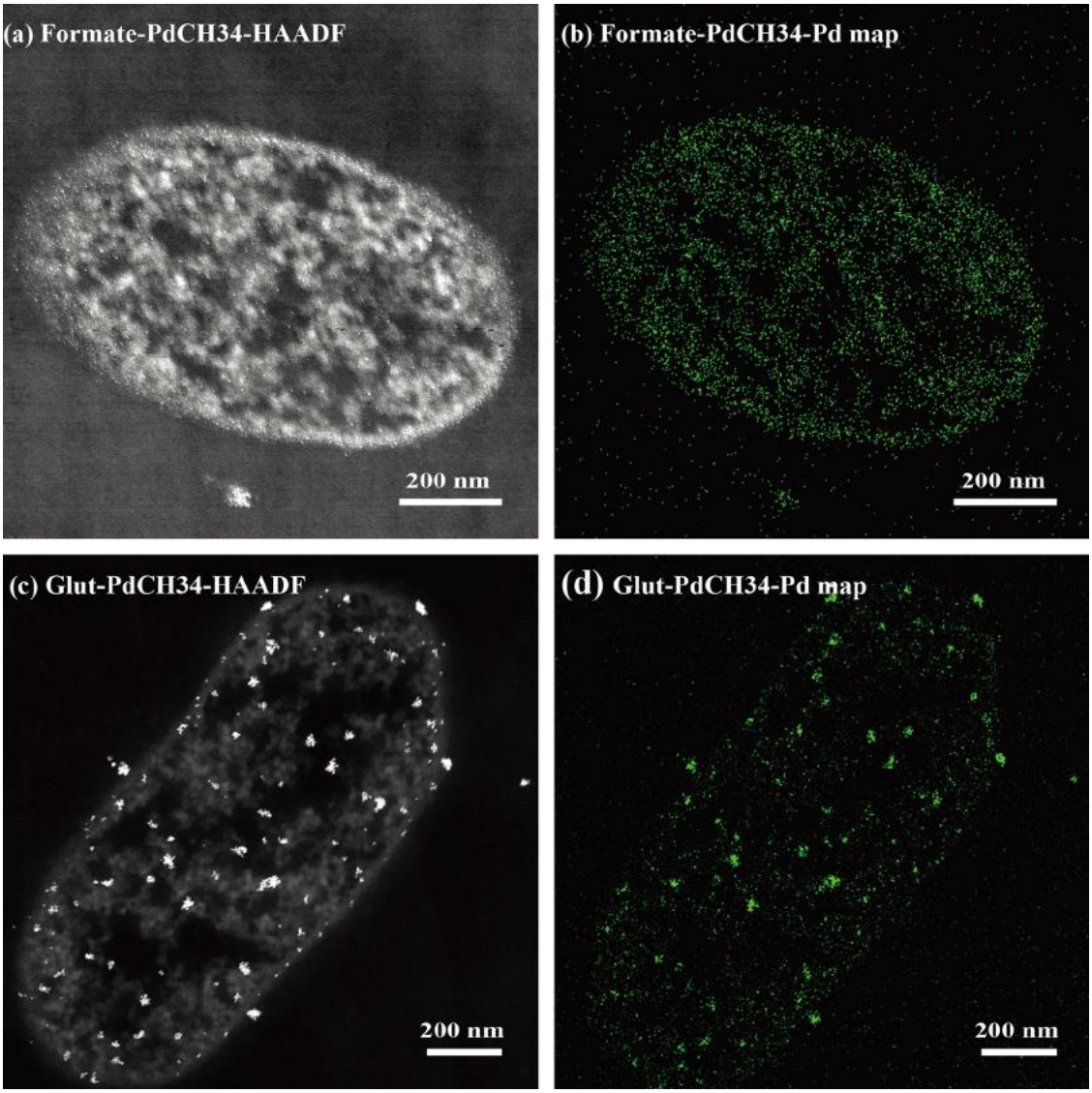

Fig. 3. Dark-field TEM images and X-ray maps of palladium for formate-PdCH34 (a, b) and glut-PdCH34 (c, d) ultra-thin sections. In plots 'a, c' cytoplasm is attributed to white pixels, and in 'b, d', the green pixels are Pd. (For interpretation of the references to color in this figure legend, the reader is referred to the web version of this article).

showed well-dispersed PdNPs mostly located in the cell envelope or inside cells associated with condensed cytoplasm (Fig. 3a and b), while most of the PdNPs in glut-PdCH34 were found in the cytoplasm (Fig. 3b and d). It should be noted that Pd(II) was also observed in association with organics constituents (cytoplasm) (Fig. 3a, b and c, d). Furthermore, the homogenous nature of PdNPs in formate-PdCH34 cells demonstrated that Pd(II) ions were stabilized in the process of formate treatment and further glutaraldehyde fixation had no effect (formate-PdCH34 was fixed using glutaraldehyde for thin section preparation). The cellular organics played a key role in the biosynthesis of PdNPs, for example, the biomolecules in bacterial biomass can provide preferential nucleation sites (Xu et al., 2018), and the metabolites could act as electron donors (formate, pyruvate and lactate) (Windt et al., 2005) and catalysts (citric acid) (Wang et al., 2012) for Pd(II) reduction.

HRTEM images of PdNPs in glutaraldehyde chemical control, formate- and glut-PdCH34 are shown in Fig. 4. The interplanar spacing of the 0.21 − 0.23 nm and 0.19 nm were in agreement with the metallic lattice fringes of face-centred cubic (fcc) Pd (1,1,1) plane with the space of 0.224 nm, and Pd (0,0,2) plane with the space of 0.194 nm (Bennett et al., 2013; Mao et al., 2014; Wang et al., 2012; Wunderlich et al., 1990). The PdNPs in glut-PdCH34 had a weaker diffraction pattern in comparison to the PdNPs in glutaraldehyde chemical control; however, SAED patterns of these two samples were identical (Fig. 4d), indicating the same crystal structure. The Bragg reflection of (1,1,1), (0,0,2), (0,2,2) and (1,1,3) further confirmed the PdNPs were polycrystalline (Kumar and Saxena, 1989). PdNPs with different structures have been synthesized using chemical and biological methods. Dendrite-shaped PdNPs covered on graphene surface were chemically synthesized, and the SAED image exhibited a diffraction pattern corresponding to (1,1,1), (2,0,0), (2,2,0) and (3,1,1) lattice facets of fcc Pd (Sahu et al., 2013). Bimetallic Pd-Cu nanoparticles synthesized with octadecylamine, were found to possess lattice fringes between fcc Pd (0.224 nm) and a Cu (0.209 nm) crystal phase in the (111) plane using HRTEM analysis (Mao et al., 2014). The biosynthesis of ultra-fine, spherical PdNPs with a size range from 2.3 to 7.5 nm was synthesized using gum ghatti (*Anogeissus latifolia*); HRTEM and SAED analyses confirmed fcc structure for PdNPs (Kora and Rastogi, 2018). Similarly, PdNPs with fcc crystal structure were synthesized by reducing the palladised *Desulfovibrio desulfuricans* biomass using H_2 (Bennett et al., 2013).

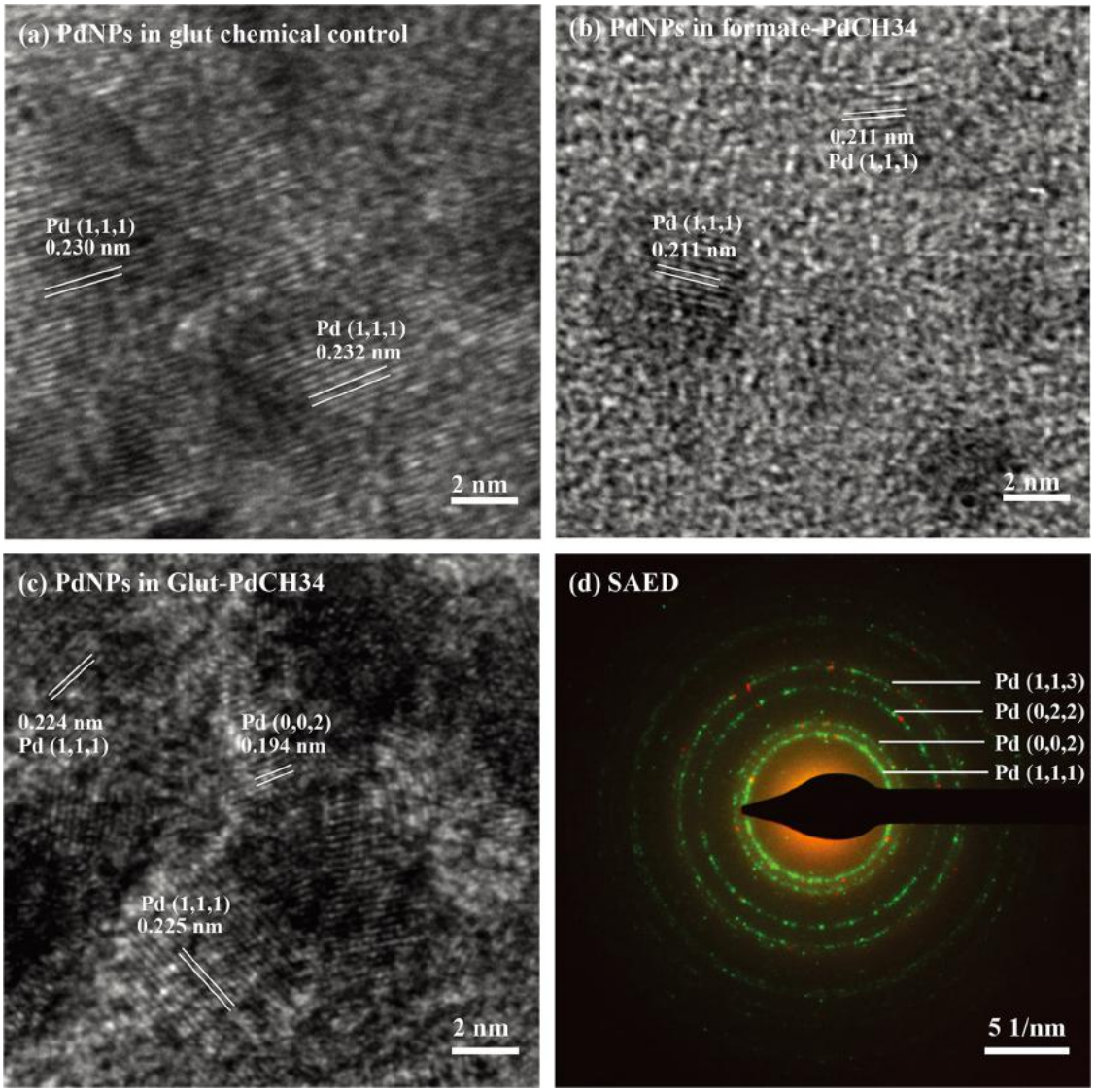

Fig. 4. High-resolution TEM images and SAED pattern for PdNPs. (a), PdNPs in the glutaraldehyde chemical control; (b), PdNPs in formate-PdCH34 ultra-thin section; (c) PdNPs in glut-PdCH34 ultra-thin section; (d) SAED pattern for PdNPs in the glutaraldehyde chemical control (green rings) and glut-PdCH34 ultra-thin section (red dots). (For interpretation of the references to color in this figure legend, the reader is referred to the web version of this article).

3.4. XPS-Pd chemical state analysis

XPS was used to evaluate the chemical state of palladium in the chemical control, PdCH34, formate-PdCH34, and glut-PdCH34 cells (Fig. 5). Survey spectra showed only palladium, oxygen and carbon in the glutaraldehyde chemical control (Fig. 5a), PdCH34 (Fig. 5c) and glut-PdCH34 (Fig. 5g), and a sodium peak in the formate-PdCH34 (Fig. 5e) consistent with ionic interactions between Pd(II) and Na(I) adsorbed by the bacterial cells (Morisada et al., 2011; Yong et al., 2002). High-resolution XPS spectra of Pd3d showed a measurable difference between inorganic chemical reactions versus organic reactions/cells. In the glutaraldehyde chemical control (Fig. 5b), double peaks with binding energies at 335.6 eV and 340.9 eV were fitted, corresponding to $Pd_{3d5/2}$ and $Pd_{3d3/2}$ of metal Pd(0) (Sun et al., 1998; Suwannarat et al., 2018; Yang et al., 2013). The binding energies of Pd (0) increased slightly (from 335.6 eV to 336.4 ± 0.2 eV and from 340.9 eV to 341.7 ± 0.2 eV) in PdCH34 (Fig. 5d), formate-PdCH34 (Fig. 5f) and glut-PdCH34 cells (Fig. 5h). The positive chemical shifts in the bacterial cells in comparison to chemical control may be attributed to several factors, including small particle size, palladium cluster compounds, and chemically bonded palladium complexes (Lengke et al., 2007; Zhou et al., 2006). The difference of supporting material in chemical control and cells could explain the positive shifts of metal Pd (0) binding energy. Golub et al. (2019) reported that the $Pd(0)_{3d5/2}$ line at 335.0 eV in unsupported bulk metal shifted to 335.8 eV in the carbon-supported sample and shifted to 336.4 eV for the melamin-based sample (Golub et al., 2019). Taking into account the adsorption system and TEM data, the second component at 338.3 ($Pd_{3d5/2}$) and 343.6 eV ($Pd_{3d3/2}$) were attributed to Pd(II), which could be derived from O-Pd-O bonds in glutaraldehyde chemical control because of the incorporation of Pd(II) in polymer cross-link process (Huang et al., 2012), and from Pd(II) adsorption by functional groups in the cells. The high Pd(II) to Pd(0) ratio shown in the Pd3d spectrum (Fig. 5d) was consistent with the dark-stained cells and a few PdNPs in TEM images of PdCH34 cells. The formate-and glut-PdCH34 cells possessed more reduced Pd(0) compared with PdCH34; however, XPS spectra revealed that all of the cells possessed more Pd(II) than Pd(0) (Fig. 5d, f and h). Two more peaks observed at 336.6 and 341.9 eV in glutaraldehyde chemical control can be attributed to Pd(II) $3d_{5/2}$ and Pd(II) $3d_{3/2}$ for PdO, which may have originated from the surface oxidation of PdNPs during the XPS sampling procedure (Celebi et al., 2016; Nyholm and Martensson, 1980).

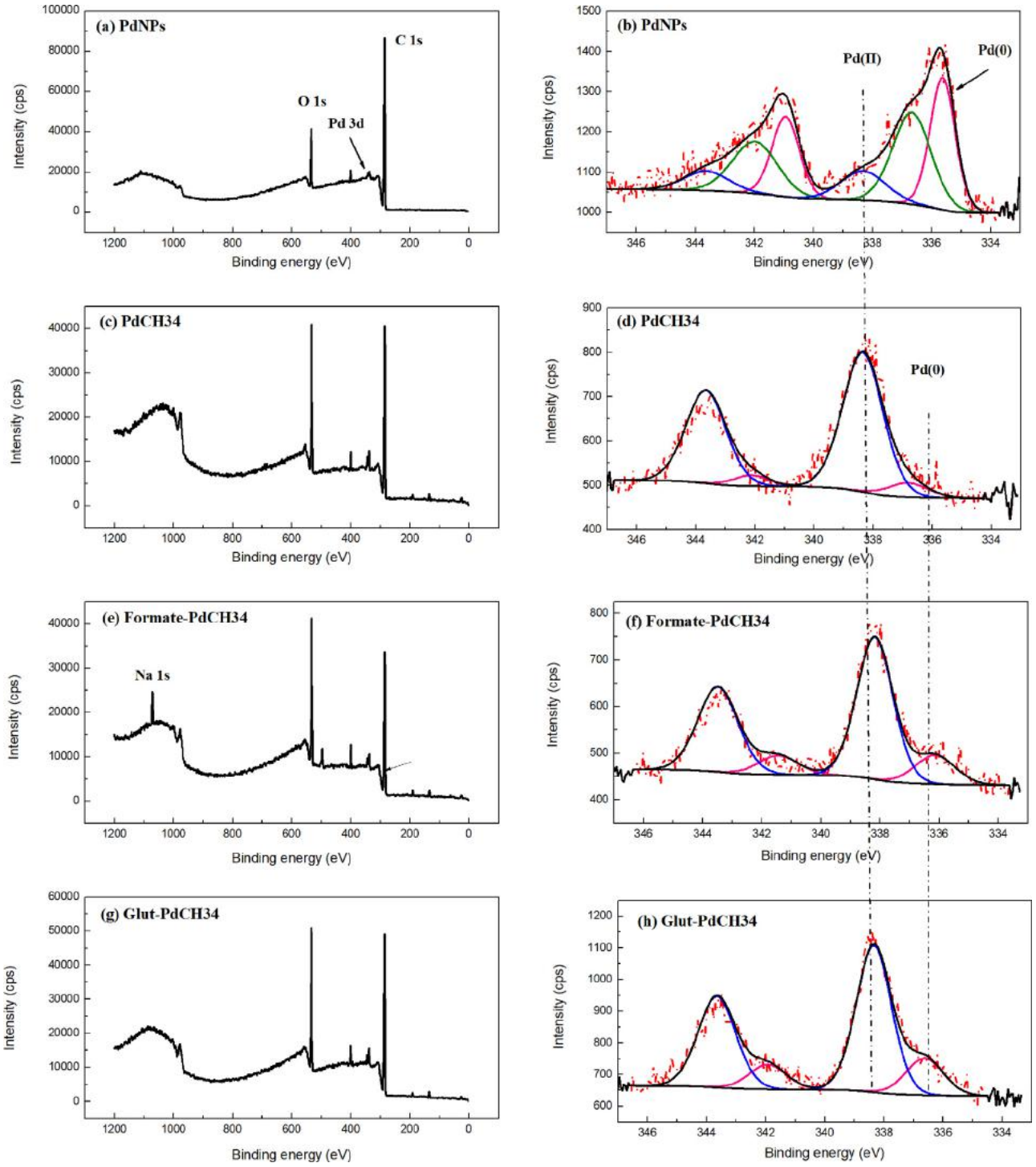

Fig. 5. XPS survey spectra and high resolution XPS spectra of Pd 3d from PdNPs in the glutaraldehyde chemical control (a, b); PdCH34 cells (c, d); formate-PdCH34 cells (e,f) and glut-PdCH34 cells (g, h).

3.5. PdNPs catalytic activity on reduction of 4-NP and Cr(VI)

The catalytic activity of PdNPs depends on several factors like particle size (Zhou et al., 2006), particle chemical state (Penner et al., 2006), the activity of facets (Fu et al., 2014) and edge/corner atoms (Huang et al., 2013). In this study, PdNPs synthesized by chemical and biological methods were used for 4-NP and Cr(VI) reduction.

In the reduction of 4-NP, the adsorption peak changed from 317 nm to 400 nm after the addition of $NaBH_4$, indicating the formation of 4-nitrophenolate ions due to the alkalinity of the solution (Dong et al., 2014). A new peak of 4-AP at 313 nm appeared as the reduction of 4-NP occurred (data not shown). As shown in Fig. 6a, blank CH34 cells showed no reduction of nitro-group with the same absorbance of pure 4-NP control, indicating that the 4-NP reduction was not possible without a metal catalyst. In PdNP-loaded bacteria, the 4-NP reduction rate showed a strong, inverse PdNP size-dependence in an order of formate-PdCH34 (< 2 nm) > PdCH34 (ca. 5 nm) > glut-PdCH34 ($10-20$ nm), although, interestingly, all three reactions 'stopped' at a removal efficiency of 92% at 110 min. The glutaraldehyde chemical control exhibited a contradictory 'reduction efficiency', between that of

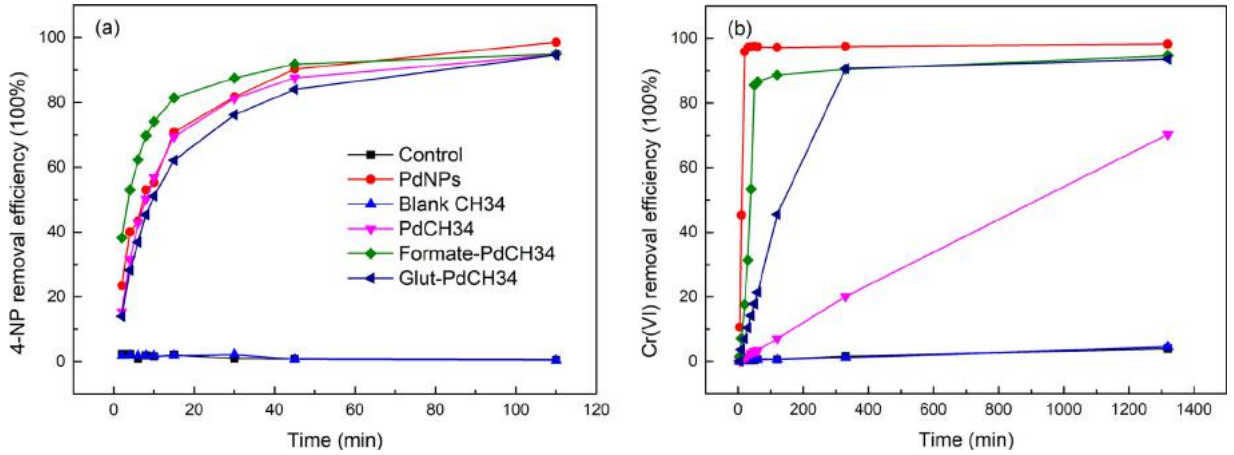

Fig. 6. Time-dependent 4-NP (a) and Cr(VI) (b) removal efficiency using different PdNPs. Same icon were shared in figures: control, reaction system without any PdNPs and cells; PdNPs, reaction system with PdNPs catalyst from glutaraldehyde chemical control; blank CH34, reaction system with blank CH34 cells; PdCH34, reaction system with PdCH34 cells; formate-PdCH34, reaction system with formate-PdCH34 cells; glut-treated, reaction system with glut-PdCH34 cells.

formate-PdCH34 and glut-PdCH34. This observation on its catalytic performance may be explained by the greater ratio of Pd(0):Pd(II) in the glutaraldehyde chemical control leading to a higher reduction efficiency than glut-PdCH34, while the larger chemical PdNPs (20 − 40 nm) resulted in a lower removal efficiency than formate-PdCH34 (< 2 nm).

The reduction of Cr(VI) to Cr(III) could be attained by using formic acid (HCOOH) as a reductant and can be improved via the catalysis of PdNPs (Omole et al., 2007). In PdNP catalysed transformations, formic acid undergoes direct mineralization to CO_2 and H_2 [$HCOOH = CO_{2(g)} + H_{2(g)}$], and then H_2 subsequently reduces Cr(VI) to Cr(III) on the surface of the PdNPs ($Cr_2O_7^{2-} + 8H^+ + 3H_{2(g)} = 2Cr^{3+} + 7H_2O$) (Celebi et al., 2016; Fu et al., 2014). No reaction was observed without a PdNP catalyst as no Cr(VI) was reduced with blank CH34 cells. Fig. 6b shows that the mass of PdNPs in the bacterial cells played a critical role in catalytic performance. A greater number of Pd(II) ions were reduced to Pd(0) in formate-PdCH34 and glut-PdCH34, resulting in a higher removal speed in comparison to PdCH34. Particle size was also a factor for Cr(VI) removal rate. It took 330 min to achieve a removal efficiency of 90% for the larger glut-PdCH34 nanoparticles versus the removal efficiency of 85% in only 50 min for formate-PdCH34. The Cr(VI) reduction in PdCH34 system possessed the slowest reaction rate but underwent a continuously steady increase with the Cr(VI) removal efficiency reaching 92% after 44 h. This result was generally consistent with that of formate- and glut-PdCH34. The chemically synthesized PdNPs showed the highest Cr(VI) removal efficiency in all PdNPs (96% at 20 min), likely because of the high Pd(0):Pd(II) ratio shown in the XPS spectrum, since the PdNPs were created using the same total amount of palladium. The Cr(VI) reduction by different PdNPs revealed that removal efficiency increased with the increase of PdNPs (catalyst) in each reaction system, and with the smaller nanoparticles enhancing catalytic performance.

The results demonstrated that the size and mass of PdNPs played an important role in 4-NP and Cr(VI) reduction and that the physical barrier of the cell membrane did not hinder the reduction process. Damage to the cell envelope during Pd(II) uptake, which would have been 'fixed' during the reaction with glutaraldehyde may have enhanced permeability, facilitating catalysis within cells. Compared with the chemically synthesized PdNP, the biosynthesized PdNP has several advantages: (1) a smaller particle size, offering more surface area for catalytic reactions, such as 4-NP and Cr(VI) reduction; (2) the bacterial biomass acts as stabiliser and disperser for PdNPs, reducing the PdNPs aggregation; (3) the adsorption of PdNPs on bacterial biomass results in a simpler reuse process since it can be done by centrifugation or filtration. Biosynthesized PdNP were comparatively active or superior to chemical PdNP in the Heck reaction, and are easily separated from the products under gravity or by filtration for reuse (6 times) with low loss or agglomeration as compared to chemical PdNP (Bennett et al., 2013).

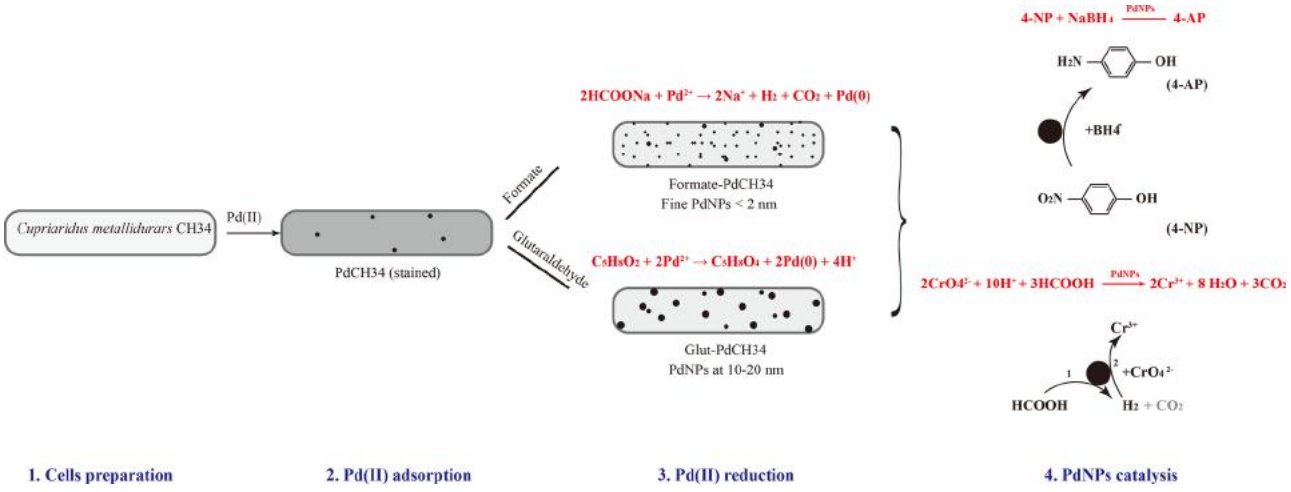

Fig. 7. Schematic illustration for adsorption, reduction of Pd(II) and catalytic reaction of PdNPs to 4-NP and Cr(VI).

4. Conclusion

A summary of the study is best depicted in Fig. 7 which illustrates the adsorption and reduction of Pd(II) in *C. metallidurans* CH34 cells and the PdNP catalysed 4-NP- and Cr(VI)-reduction. In the Pd(II) adsorption process, most of the Pd(II) ions are bound to cell organics producing metal stained bacteria, with a small amount of Pd(II) ions reduced to Pd(0) forming PdNPs. The Pd(II) adsorbed by the cell constituents could be reduced to Pd(0) by the addition of reductant fixatives, such as formate and glutaraldehyde. Fine PdNPs (< 2 nm) formed after the formate treatment, while PdNPs between $10-20$ nm formed with glutaraldehyde treatment. An increased ratio of Pd(0):Pd(II) occurred in the PdCH34 cells after formate or glutaraldehyde reduction, and the highest PdNP Pd ratio was found in the chemical glutaraldehyde control. The size and mass of PdNPs played an important role in the catalytic reaction, specifically, the small PdNPs in formate-PdCH34 performed best with 4-NP and Cr(VI) reduction compared to the PdNPs in glut-PdCH34; the highest Cr(VI) removal efficiency occurred in chemically formed PdNPs due to the highest PdNP ratio compared with formate- and glut-PdCH34 cells. In summary, glutaraldehyde, a routine fixative used in the preparation of bacterial ultra-thin sections could reduce cell-adsorbed Pd(II) to Pd(0), generating PdNP 'artefacts' in TEM. Thus the capability of Pd(II) reduction by bacteria would be overestimated when using ultra-thin sections (fixatives to preserve cells) to observe PdNPs in bacteria.

CRediT authorship contribution statement

Ling Tan: Writing - original draft. **Thomas Ray Jones:** Writing - review & editing. **Jordan Poitras:** Writing - review & editing. **Jianping Xie:** Funding acquisition, Writing - review & editing, Supervision. **Xinxing Liu:** Formal analysis, Writing - review & editing. **Gordon Southam:** Funding acquisition, Conceptualization, Writing - review & editing, Supervision.

Declaration of Competing Interest

None.

Acknowledgements

The authors acknowledge the facilities, the scientific and technical assistance, of the Australian Microscopy & Microanalysis Research Facility at the Centre for Microscopy and Microanalysis, The University of Queensland. We thank Han Gao for the assistant of SAED analysis. We thank the five, anonymous reviews for their constructive comments that have improved the presentation of this work. This work was supported by the Australian Research Council Linkage Program to G. Southam (LP140100804), National Natural Science Foundation of China (51871250), and also supported by Chinese Scholarship Council (CSC) Scholarship to Ling Tan.

References

Bennett, J., Mikheenko, I., Deplanche, K., Shannon, I., Wood, J., Macaskie, L., 2013. Nanoparticles of palladium supported on bacterial biomass: New re-usable heterogeneous catalyst with comparable activity to homogeneous colloidal Pd in the Heck reaction. Appl. Catal. B-Environ. 140, 700–707.

Campbell, G., MacLean, L., Reith, F., Brewe, D., Gordon, R., Southam, G., 2018. Immobilisation of platinum by*Cupriavidus metallidurans*. Minerals 8, 10.

Celebi, M., Yurderi, M., Bulut, A., Kaya, M., Zahmakiran, M., 2016. Palladium nanoparticles supported on amine-functionalized SiO_2 for the catalytic hexavalent chromium reduction. Appl. Catal. B-Environ. 180, 53–64.

Chen, X., Wu, G., Chen, J., Chen, X., Xie, Z., Wang, X., 2011. Synthesis of "clean" and well-dispersive Pd nanoparticles with excellent electrocatalytic property on graphene oxide. J. Am. Chem. Soc. 133, 3693–3695.

Chiou, J.R., Lai, B.H., Hsu, K.C., Chen, D.H., 2013. One-pot green synthesis of silver/iron oxide composite nanoparticles for 4-nitrophenol reduction. J. Hazard. Mater. 248-249, 394–400.

Cookson, J., 2012. The preparation of palladium nanoparticles. Platinum Met. Rev. 56, 83–98.

Coupland, R., Hopwood, D., 1966. The mechanism of the differential staining reaction for adrenaline-and noreadrenaline-storing granules in tissues fixed in glutaraldehyde. J. Anat. 100, 227.

Creamer, N., Mikheenko, I., Yong, P., Deplanche, K., Sanyahumbi, D., Wood, J., Pollmann, K., Merroun, M., Selenska-Pobell, S., Macaskie, L., 2007. Novel supported Pd hydrogenation bionanocatalyst for hybrid homogeneous/heterogeneous catalysis. Catal. Today 128, 80–87.

Cui, J., Zhu, N., Kang, N., Ha, C., Shi, C., Wu, P., 2017. Biorecovery mechanism of palladium as nanoparticles by *Enterococcus faecalis*: From biosorption to bioreduction. Chem. Eng. J. 328, 1051–1057.

Dai, S., Wu, X., Zhang, J., Fu, Y., Li, W., 2018. Coenzyme A-regulated Pd nanocatalysts for formic acid-mediated reduction of hexavalent chromium. Chem. Eng. J. 351, 959–966.

De Windt, W., Boon, N., Van den Bulcke, J., Rubberecht, L., Prata, F., Mast, J., Hennebel, T., Verstraete, W., 2006. Biological control of the size and reactivity of catalytic Pd (0) produced by *Shewanella oneidensis*. Antonie Van Leeuwenhoek 90, 377–389.

Deplanche, K., Caldelari, I., Mikheenko, I.P., Sargent, F., Macaskie, L.E., 2010. Involvement of hydrogenases in the formation of highly catalytic Pd (0) nanoparticles by bioreduction of Pd (II) using *Escherichia coli* mutant strains. Microbiology 156, 2630–2640.

Dong, Z., Le, X., Liu, Y., Dong, C., Ma, J., 2014. Metal organic framework derived magnetic porous carbon composite supported gold and palladium nanoparticles as highly efficient and recyclable catalysts for reduction of 4-nitrophenol and hydrodechlorination of 4-chlorophenol. J. Mater. Chem. A Mater. Energy Sustain. 2, 18775–18785.

Feng, Y., Yu, Y., Wang, Y., Lin, X., 2007. Biosorption and bioreduction of trivalent aurum by photosynthetic bacteria *Rhodobacter capsulatus*. Curr. Microbiol. 55, 402–408.

Froehlich, P., Lorenz, T., Martin, G., Brett, B., Bertau, M., 2017. Valuable metals-recovery processes, current trends, and recycling strategies. Angew. Chemie Int. Ed. Engl. 56, 2544–2580.

Fu, G.T., Jiang, X., Wu, R., Wei, S.H., Sun, D.M., Tang, Y.W., Lu, T.H., Chen, Y., 2014. Arginine-assisted synthesis and catalytic properties of single-crystalline palladium tetrapods. ACS Appl. Mater. Interfaces 6, 22790–22795.

Gao, Y., Sun, W., Yang, W., Li, Q., 2018. Palladium nanoparticles supported on amine-functionalized glass fiber mat for fixed-bed reactors on the effective removal of hexavalent chromium by catalytic reduction. J. Mater. Sci. Technol. 34, 961–968.

Gillett, R., Gull, K., 1972. Glutaraldehyde - its purity and stability. Histochemie 30, 162–167.

Golub, F.S., Beloshapkin, S., Gusel'nikov, A.V., Bolotov, V.A., Parmon, V.N., Bulushev, D.A., 2019. Boosting hydrogen production from formic acid over Pd catalysts by deposition of N-containing precursors on the carbon support. Energies 12, 3885.

Huang, Y., Ma, H., Wang, S., Shen, M., Guo, R., Cao, X., Zhu, M., Shi, X., 2012. Efficient catalytic reduction of hexavalent chromium using palladium nanoparticle-immobilized electrospun polymer nanofibers. ACS Appl. Mater. Interfaces 4, 3054–3061.

Huang, X., Li, Y., Chen, Y., Zhou, E., Xu, Y., Zhou, H., Duan, X., Huang, Y., 2013. Palladium-based nanostructures with highly porous features and perpendicular pore channels as enhanced organic catalysts. Angew. Chem. Int. Ed. 52, 2520–2524.

Kora, A.J., Rastogi, L., 2018. Green synthesis of palladium nanoparticles using gum ghatti (*Anogeissus latifolia*) and its application as an antioxidant and catalyst. Arab. J. Chem. 11, 1097–1106.

Kumar, J., Saxena, R., 1989. Formation of NaCl-and Cu_2O-type oxides of platinum and palladium on carbon and alumina support films. J. Less Common Met. 147, 59–71.

Le, X., Dong, Z., Liu, Y., Jin, Z., Huy, T.-D., Le, M., Ma, J., 2014. Palladium nanoparticles immobilized on core-shell magnetic fibers as a highly efficient and recyclable heterogeneous catalyst for the reduction of 4-nitrophenol and Suzuki coupling reactions. J. Mater. Chem. A Mater. Energy Sustain. 2, 19696–19706.

Le, X., Dong, Z., Li, X., Zhang, W., Le, M., Ma, J., 2015. Fibrous nano-silica supported palladium nanoparticles: An efficient catalyst for the reduction of 4-nitrophenol and hydrodechlorination of 4-chlorophenol under mild conditions. Catal. Commun. 59, 21–25.

Ledrich, M.L., Stemmler, S., Laval-Gilly, P., Foucaud, L., Falla, J., 2005. Precipitation of silver-thiosulfate complex and immobilization of silver by *Cupriavidus metallidurans* CH34. Biometals 18, 643–650.

Lee, J.T.Y., Chow, K.L., 2012. SEM sample preparation for cells on 3D scaffolds by freeze-drying and HMDS. Scanning 34, 12–25.

Lengke, M.F., Fleet, M.E., Southam, G., 2007. Synthesis of palladium nanoparticles by reaction of filamentous cyanobacterial biomass with a palladium (II) chloride complex. Langmuir 23, 8982–8987.

Leopold, K., Maier, M., Weber, S., Schuster, M., 2008. Long-term study of palladium in road tunnel dust and sewage sludge ash. Environ. Pollut. 156, 341–347.

Leopold, K., Wörle, K., Schindl, R., Huber, L., Maier, M., Schuster, M., 2017. Determination of traffic-related palladium in tunnel dust and roadside soil. Sci. Total Environ. 583, 169–175.

Leśniewska, B.A., Godlewska-Żyłkiewicz, B., Bocca, B., Caimi, S., Caroli, S., Hulanicki, A., 2004. Platinum, palladium and rhodium content in road dust, tunnel dust and common grass in Białystok area (Poland): a pilot study. Sci. Total Environ. 321, 93–104.

Li, S., Li, H., Liu, J., Zhang, H., Yang, Y., Yang, Z., Wang, L., Wang, B., 2015. Highly efficient degradation of organic dyes by palladium nanoparticles decorated on 2D magnetic reduced graphene oxide nanosheets. Dalton Trans. 44, 9193–9199.

Mao, J., Liu, Y., Chen, Z., Wang, D., Li, Y., 2014. Bimetallic Pd–Cu nanocrystals and their tunable catalytic properties. Chem. Commun. (Camb.) 50, 4588–4591.

Mazumder, V., Sun, S., 2009. Oleylamine-mediated synthesis of Pd nanoparticles for

catalytic formic acid oxidation. J. Am. Chem. Soc. 131, 4588–4589.
Mikheenko, I., Gomez-Bolivar, J., Merroun, M., Sharma, S., Macaskie, L., 2016. High resolution electron microscopy study of biologically derived ruthenium and palladium/ruthenium nanoparticles. In: Proceedings of the International Conference on Nanomaterials: Application & Properties (NAP), 2016. P. 01NNPT03-1-01NNPT03-4.
Monchy, S., Benotmane, M.A., Janssen, P., Vallaeys, T., Taghavi, S., Van Der Lelie, D., Mergeay, M., 2007. Plasmids pMOL28 and pMOL30 of *Cupriavidus metallidurans* are specialized in the maximal viable response to heavy metals. J. Bacteriol. 189, 7417–7425.
Montero-Silva, F., Durán, N., Seeger, M., 2017. Synthesis of extracellular gold nanoparticles using *Cupriavidus metallidurans* CH34 cells. IET Nanobiotechnol. 12, 40–46.
Morisada, S., Kim, Y.H., Ogata, T., Marutani, Y., Nakano, Y., 2011. Improved adsorption behaviors of amine-modified tannin gel for palladium and platinum ions in acidic chloride solutions. Ind. Eng. Chem. Res. 50, 1875–1880.
Ncube, P., Bingwa, N., Baloyi, H., Meijboom, R., 2015. Catalytic activity of palladium and gold dendrimer-encapsulated nanoparticles for methylene blue reduction: a kinetic analysis. Appl. Catal. A Gen. 495, 63–71.
Ng, C.K., Karahan, H.E., Loo, S.C.J., Chen, Y., Cao, B., 2019. Biofilm-templated heteroatom-doped carbon-palladium nanocomposite catalyst for hexavalent chromium reduction. A ACS Appl. Mater. Interfaces 11, 24018–24026.
Nyholm, R., Martensson, N., 1980. Core level binding energies for the elements Zr-Te (Z = 40–52). J. Phys. C: Solid State Phys. 13, 279–284.
Omole, M.A., K'Owino, I.O., Sadik, O.A., 2007. Palladium nanoparticles for catalytic reduction of Cr (VI) using formic acid. Appl. Catal. B-Environ. 76, 158–167.
Penner, S., Wang, D., Jenewein, B., Gabasch, H., Klötzer, B., Knop-Gericke, A., Schlögl, R., Hayek, K., 2006. Growth and decomposition of aligned and ordered PdO nanoparticles. J. Chem. Phys. 125, 094703.
Sabatini, D.D., Bensch, K., Barrnett, R.J., 1963. Cytochemistry and electron microscopy: the preservation of cellular ultrastructure and enzymatic activity by aldehyde fixation. J. Cell Biol. 17, 19–58.
Sahu, S.C., Samantara, A.K., Dash, A., Juluri, R., Sahu, R.K., Mishra, B., Jena, B.K., 2013. Graphene-induced Pd nanodendrites: a high performance hybrid nanoelectrocatalyst. Nano Res. 6, 635–643.
Saldan, I., Semenyuk, Y., Marchuk, I., Reshetnyak, O., 2020. Chemical synthesis and application of palladium nanoparticles. J. Mater. Sci. 50, 2337–2354.
Srivastava, N., Mukhopadhyay, M., 2015. Ralstonia eutropha (*Cupriavidus metallidurans*) mediated biosynthesis of gold nanoparticles and catalytic treatment of 2, 4 dichlorophenol. Synth. React. Inorg. Metals 45, 238–247.
Sun, R., Tryk, D., Hashimoto, K., Fujishima, A., 1998. Formation of catalytic Pd on ZnO thin films for electroless metal deposition. J. Electrochem. Soc. 145, 3378–3382.
Suwannarat, K., Thongthai, K., Ananta, S., Srisombat, L., 2018. Synthesis of hollow trimetallic Ag/Au/Pd nanoparticles for reduction of 4-nitrophenol. Colloids Surf. Physicochem. Eng. Asp. 540, 73–80.
Tan, L., Dong, H., Liu, X., He, J., Xu, H., Xie, J., 2017. Mechanism of palladium (II) biosorption by *Providencia vermicola*. RSC Adv. 7, 7060–7072.
Tilch, J., Schuster, M., Schwarzer, M., 2000. Determination of palladium in airborne particulate matter in a German city. Fresen. J. Anal. Chem. 367, 450–453.
Wang, Z.L., Yan, J.M., Wang, H.L., Ping, Y., Jiang, Q., 2012. Pd/C synthesized with citric acid: an efficient catalyst for hydrogen generation from formic acid/sodium formate. Sci. Rep. 2, 598.
Whipple, E.B., Ruta, M., 1974. Structure of aqueous glutaraldehyde. J. Org. Chem. 39, 1666–1668.
Windt, W.D., Aelterman, P., Verstraete, W., 2005. Bioreductive deposition of palladium (0) nanoparticles on *Shewanella oneidensis* with catalytic activity towards reductive dechlorination of polychlorinated biphenyls. Environ. Microbiol. 7, 314–325.
Wu, X., Lu, C., Zhang, W., Yuan, G., Xiong, R., Zhang, X., 2013. A novel reagentless approach for synthesizing cellulose nanocrystal-supported palladium nanoparticles with enhanced catalytic performance. J. Mater. Chem. 1, 8645–8652.
Wunderlich, W., Ishida, Y., Maurer, R., 1990. HREM-studies of the microstructure of nanocrystalline palladium. Scr. Metal. Mater. 24, 403–408.
Xu, H., Xiao, Y., Xu, M., Cui, H., Tan, L., Feng, N., Liu, X., Qiu, G., Dong, H., Xie, J., 2018. Microbial synthesis of Pd-Pt alloy nanoparticles using *Shewanella oneidensis* MR-1 with enhanced catalytic activity for nitrophenol and azo dyes reduction. Nanotechnology. 30, 065607.
Yang, X., Zhen, M., Li, G., Liu, X., Wang, X., Shu, C., Jiang, L., Wang, C., 2013. Preparation of Pd-decorated fullerenols on carbon nanotubes with excellent electrocatalytic properties in alkaline media. J. Mater. Chem. A Mater. Energy Sustain. 1, 8105–8110.
Yates, M.D., Cusick, R.D., Logan, B.E., 2013. Extracellular palladium nanoparticle production using *Geobacter sulfurreducens*. ACS Sustain. Chem. Eng. 1, 1165–1171.
Yong, P., Rowson, N.A., Farr, J.P.G., Harris, I.R., Macaskie, L.E., 2002. Bioaccumulation of palladium by *Desulfovibrio desulfuricans*. J. Chem. Technol. Biotechnol. 77, 593–601.
Yuan, P., Liu, D., Fan, M., Yang, D., Zhu, R., Ge, F., Zhu, J., He, H., 2010. Removal of hexavalent chromium [Cr (VI)] from aqueous solutions by the diatomite-supported/unsupported magnetite nanoparticles. J. Hazard. Mater. 173, 614–621.
Zhou, W.P., Lewera, A., Larsen, R., Masel, R.I., Bagus, P.S., Wieckowski, A., 2006. Size effects in electronic and catalytic properties of unsupported palladium nanoparticles in electrooxidation of formic acid. J. Phys. Chem. B 110, 13393–13398.